1-1-2013

Non-local coherent coupling between excitons in a disordered quantum well

Yuri D. Glinka

Mikhail Erementchouk
University of Central Florida

Chandriker K. Dass

Michael N. Leuenberger
University of Central Florida

Allan S. Bracker

See next page for additional authors

PAPER • OPEN ACCESS

Non-local coherent coupling between excitons in a disordered quantum well

New Journal of Physics
The open access journal for physics

Non-local coherent coupling between excitons in a disordered quantum well

Yuri D Glinka[1,2], Mikhail Erementchouk[3], Chandriker K Dass[1], Michael N Leuenberger[3], Allan S Bracker[4] and Xiaoqin Li[1,5]

[1] Physics Department, University of Texas, Austin, TX 78712, USA
[2] Institute of Physics, National Academy of Sciences of Ukraine, Kiev 03028, Ukraine
[3] NanoScience Technology Center and Department of Physics, University of Central Florida, Orlando, FL 32826, USA
[4] Naval Research Laboratory, Washington, DC 20375 USA
E-mail: elaineli@physics.utexas.edu

New Journal of Physics **15** (2013) 075026 (12pp)
Received 3 April 2013
Published 26 July 2013
Online at http://www.njp.org/
doi:10.1088/1367-2630/15/7/075026

Abstract. We investigated coherent coupling among multiple exciton resonances formed in a single disordered quantum well using the powerful electronic two-dimensional Fourier transform spectroscopy. Our experiment revealed clear signatures of non-local coherent coupling between the heavy-hole and light-hole excitons residing in regions that differ in thickness by one atomic layer. The experimental observation is qualitatively explained by spatial overlap between exciton linear response functions calculated within a single defect model.

[5] Author to whom any correspondence should be addressed.

Contents

In direct-gap semiconductor heterostructures such as quantum wells (QWs), quantum wires and quantum dots, the optical response at low temperature is dominated by excitons (bound electron–hole pairs). Many-body interactions among optically excited excitons have been extensively investigated using optical coherent nonlinear spectroscopy techniques such as transient differential transmission and four-wave mixing (FWM) [1, 2]. Various spectroscopic signatures have been identified and attributed to Coulomb correlation among excitons. Such spectroscopy signatures include coherent nonlinear signal at the 'wrong' delays [3], a slow rise time [4] and excitation power-dependent dephasing time [5] or spectral shift [6]. Quite often, the microscopic origins of such spectroscopy signatures are difficult to identify and distinguish from each other.

The recent development of optical two-dimensional Fourier transform spectroscopy (2DFTS) is a welcome addition to the tool set of coherent nonlinear spectroscopy [7–9]. The ability to detect the phase evolution of a weak, nonlinear signal field and correlate such phase evolution in several time periods allows one to separate the complex quantum mechanical paths and to isolate contributions from individual terms in the density matrix that describes the open quantum system under investigation. In 2DFTS, the signatures of excitation-induced dephasing and excitation-induced shift become distinct and easy to identify [10]. Using 2DFTS, one can also probe 'dark transitions' via the modified phase evolution even though their direct dipole coupling to the excitation or radiation field is forbidden by the optical selection rules [11, 12]. 2DFTS is particularly powerful in identifying couplings among several simultaneously excited electronic transitions [13, 14]. The study reported in this paper is one such example.

In semiconductor QWs, the confinement potential in the growth direction lifts the degeneracy between the heavy-hole (HH) and light-hole (LH) excitons. Excitation pulses with a bandwidth broad enough to cover both transitions lead to oscillations in the optical response. Such HH- and LH-exciton beats have been investigated extensively because of their technical relevance in generating THz radiation [15] as well as their role in elucidating many-body interactions among excitons [16–20]. In disordered QWs, quantum beats with periods distinct from the HH and LH energy separation have been observed in the past and attributed to couplings among HH excitons formed in regions of different QW thickness due to monolayer fluctuations at the interfaces [17, 21–24]. However, conflicting conclusions are often drawn from these previous experiments, and coherent coupling among excitons in disordered QWs remains a controversial subject. The origin of quantum beats in a disordered QW is difficult to identify using traditional spectroscopy methods, partially due to the limited

temporal and spectral information accessible and partially due to the insufficient control of the interface morphology. Coherent coupling among excitons plays a key role in energy transfer processes in semiconductor heterostructures [25] and other interesting physical systems such as photosynthesis [26–28]. Understanding coherent coupling and incoherent energy transfer among multiple electronic transitions, especially in the presence of disorder, remains a great intellectual challenge relevant for optoelectronics and light-harvesting applications.

HH–LH coupling between excitons localized in the same region of a QW is expected and has been extensively investigated using 2DFT spectroscopy [10, 29, 30] as well as traditional spectroscopy methods. In this paper, we focus on whether HH and LH excitons localized in different regions in a disordered QW are coupled. Using optical 2DFTS, our experiment showed that non-local, coherent coupling between HH and LH excitons exists even when such couplings between the same type of excitons (i.e. HH–HH or LH–LH) are absent. Calculations based on a single defect model qualitatively reproduced the experimental observation.

1. Exciton resonances in a perfect QW versus a disordered one

In QWs, quantum confinement in the growth direction lifts the degeneracy of the HH and LH valence bands, which are distinguished by their angular moments of $3/2$ and $1/2$, respectively. Several optical transitions allowed by the selection rules in the electron–hole representation are illustrated in figure 1(a). In a perfect QW, only two resonances corresponding to HH and LH excitons are spectrally resolved, both being twofold spin degenerate. These resonances are plotted in the excitation picture, as shown in figure 1(b). In a disordered QW, there are monolayer fluctuations at the interfaces. The QW width fluctuations are discrete, in steps of one atomic layer. The change in exciton resonance introduced by the thickness fluctuations is most pronounced in narrow QWs where the ratio of the thickness of the single atomic layer to the QW width is appreciable. In addition, lateral dimensions of the monolayer fluctuations vary and result in further inhomogeneous broadening. If the energy splitting for excitons residing in different QW thickness regions is larger than the homogeneous and inhomogeneous linewidth of excitons, additional resonances appear in the linear spectra [31–34]. We only discuss two types of excitons relevant to the focus of the current paper: HH (LH) excitons residing in the wider and average thickness regions of the QW, which are referred to as HH_w (LH_w) and HH_a (LH_a), respectively, and are illustrated in figure 1(c). It is possible to observe additional exciton resonances in regions narrower than the average QW thickness or regions that differ by two or even three monolayers in thickness from the average QW thickness [34].

We now discuss the conditions under which the excitons due to the monolayer fluctuations may be spectrally resolved. Qualitative features of the linear optical spectrum in the presence of interface disorder are determined by the relation between two characteristic length scales: the disorder correlation length r_c and the confinement length ξ_0. Physically, r_c approximately describes the size of a typical island, and ξ_0 is the critical island size above which an exciton localized inside that island has a kinetic energy less than its potential energy. The localization length is defined as $\xi_0 = \pi\hbar\sqrt{2MV_0}$, where M is the exciton reduced mass and V_0 is the potential energy arising from the fluctuation in the QW thickness. If the typical size of islands, r_c, is larger than the localization length, ξ_0, the optical spectrum exhibits doublets. If the typical island size r_c is much smaller than the localization length ξ_0, the excitons average over the fluctuating potential and the optical spectrum exhibits a single resonance. This qualitative picture is illustrated by results of numerical simulations of the linear optical response presented

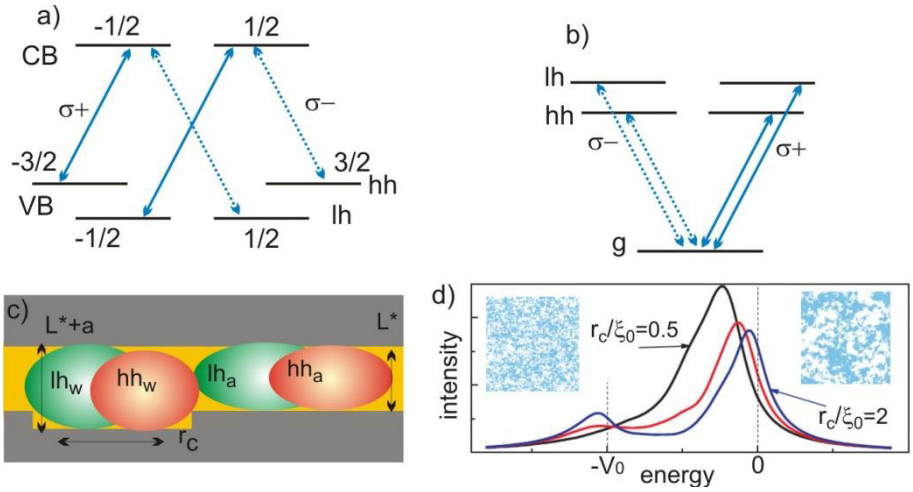

Figure 1. Level diagrams of optical transitions, sample illustration and the simulated linear optical spectra in a disordered QW. (a) Dipole-allowed HH and LH transitions in the electron–hole picture; (b) HH and LH excitons in the excitation picture; (c) HH and LH excitons in the presence of one monolayer thickness fluctuation. (d) Simulated linear optical spectra of HH (or LH) excitons suggest that a homogeneous broadened exciton resonance splits into a doublet when the disorder correlation length r_c becomes larger than the confinement length ξ_0. Insets in (d) are maps of the disorder potential used in the simulation for the case of $r_c/\xi_0 = 0.5$ (left) and 2 (right).

in figure 1(d), where the magnitude of the exciton linear polarization induced by an incoming plane wave is plotted as a function of energy for different cases corresponding to different relations between r_c and length ξ_0.

2. Identifying relevant exciton resonances experimentally

The GaAs/AlGaAs QW sample under investigation was grown by molecular beam epitaxy on semi-insulating GaAs(100) substrates. A series of four single QWs of different widths (nominally 4.2, 6.2, 8.4 and 14.0 nm) was grown with 40 nm $Al_{0.3}Ga_{0.7}As$ barriers between them. Two-minute growth interrupts at the hetero-interfaces were introduced during growth and led to the formation of large monolayer islands with lateral dimensions of approximately tens of nanometers. The average laser power of 3–5 mW used in our experiments created excitons with a sheet density of $\sim 10^{10}$ cm^{-2}. At this high excitation power, excitation-induced dephasing [5, 35] may contribute significantly to the homogeneous line width of the exciton resonances. The sample was held at 4.2 K for all optical experiments.

We identify relevant exciton resonances via photoluminescence (PL) and FWM spectra displayed in figures 2(a) and (b), respectively. The PL spectra are dominated by the HH resonances while both HH and LH resonances are present in the FWM spectra. The LH excitons are clearly observed and labeled for QWs with nominal thickness of 6.2, 8.4 and 14 nm in figure 2(b). The LH excitons in the 4.2 nm QW are shifted to higher energy outside the excitation bandwidth (not shown). HH and LH resonances are further split to two or three resonances,

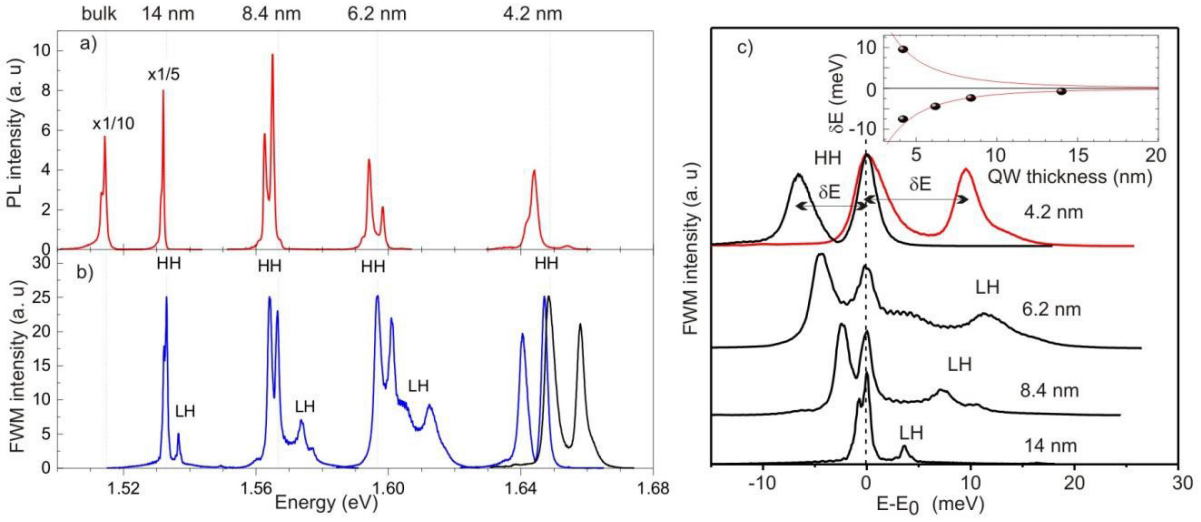

Figure 2. Identifying exciton resonances via comparison between PL and FWM spectra and analysis of the FWM spectra. (a) PL spectra for QWs with different thickness. Only HH excitons are observed in the PL spectra. (b) Both HH and LH excitons are present in the FWM spectra. (c) Shifted FWM spectra. E_0 corresponds to the HH exciton energies in the average thickness regions in the QWs. LH resonances are labeled explicitly in all QWs except for the 4.2 nm QW, in which the LH excitons are shifted to higher energies. The inset is the HH exciton energy splitting (δE) due to the monolayer thickness fluctuations as a function of the QWs. In the case of the 4.2 nm QW, two curves present in both (b) and (c) are taken with different wavelength tunings of the excitation pulses.

which originate from the monolayer fluctuations in the thickness of the QW. Identifying these multiple resonances is not a trivial task. A good approach is to investigate the systematic change of the monolayer splitting as a function of the QW width. We initially make the reasonable assumption that the lowest energy peak in the FWM spectra for each QW originates from HH_w excitons, i.e. excitons residing at the wider QW regions. We then replot HH resonances in FWM spectra (figure 2(c)) as a function of the relative energy $\delta E = (E - E_0)$, where E_0 specifies the energy for HH excitons residing in regions of average QW thickness (i.e. HH_a). Negative δE corresponds to excitons residing in wider-width disorders while positive δE corresponds to excitons formed near narrower-width disorder. We plot δE as a function of the QW thickness in the inset of figure 2(c). Within the effective mass approximation, δE, due to monolayer fluctuation of the QW width ($\delta L^* = \pm a$), is given as follows:

$$\delta E = \frac{h^2\pi^2}{2\mu_{\mathrm{HH}}}\left(\frac{1}{(L^* \mp a)^2} - \frac{1}{L^{*2}}\right) \approx -\frac{h^2\pi^2\delta L^*}{\mu_{\mathrm{HH}}L^{*3}}, \tag{1}$$

where $L^* = L + 2\Lambda$ denotes an enlargement of the QW width owing to an average wave function penetration depth into the $Al_{0.3}Ga_{0.7}As$ barrier ($\Lambda = 1.5$ nm) [36]. We first extracted the in-plane reduced exciton mass $\mu_{\mathrm{HH}} = 0.055m_e$ from the dependence of E_0 on QW width (not shown explicitly). We then fitted the data in the inset of figure 2(c) using equation (1) to obtain $a = 0.25$ nm, which matches the known value for the thickness of one atomic monolayer in GaAs. This analysis strongly supports our identification of different types of excitons.

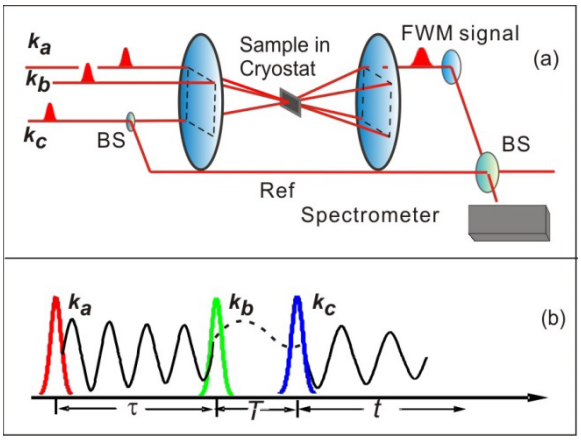

Figure 3. Experimental setup schematics and the pulse sequence used in the rephrasing experiments.

We note that trions [37] or excitonic excited states [38] have different binding energies and cannot account for the resonances observed in our experiments. The rest of the paper is focused on 2DFTS experiments performed on the 8.4 nm thick QW in which we observed interesting non-local coupling between HH and LH excitons.

3. 2DFTS experiments and results

The experimental setup for 2DFTS (figure 3(a)) employed has been described in detail elsewhere [39]. Briefly, three collinearly polarized, phase-stabilized excitation pulses with wave vectors $\boldsymbol{k}_a$, $\boldsymbol{k}_b$ and $\boldsymbol{k}_c$ have been arranged in a box geometry, generating the FWM signal in the phase-matched direction: $\boldsymbol{k}_s = -\boldsymbol{k}_a + \boldsymbol{k}_b + \boldsymbol{k}_c$. The FWM signal is then heterodyne detected with a reference beam that bypasses the sample. The reference beam is phase stabilized with other excitation pulses. By taking spectral interferograms between the reference beam and the FWM signal, we retrieve the phase information of the FWM signal.

For the rephasing pulse sequence chosen for the experiments reported here, the conjugated pulse $\boldsymbol{k}_a$ arrives first and the pulse $\boldsymbol{k}_c$ arrives last. The time periods between three excitation pulses are denoted as the evolution time τ, the waiting time T and the detection time t, respectively, as illustrated in figure 3(b). The phase of the FWM evolves as $e^{-i(\omega_\tau \tau - \omega_t t)}$ for the rephasing pulse sequence. While we only detect the nonlinear signal field in the detection time period, the initial phase at $t = 0$ carries information about the polarization field created in the evolution period. By taking phase resolved FWM signal at different τ delays with $\sim (1/100)\lambda$ precision, one can monitor and correlate nonlinear polarization phase evolution during two independent periods, τ and t, separated by the waiting time T.

Unique to 2DFTS, a quantum mechanical pathway that corresponds to absorption at one frequency ω_τ and emission at a different frequency ω_t leads to a cross-peak in the 2D spectrum. Such spectroscopic features unambiguously identify coupling between two resonances. Furthermore, by examining the ratio between the intensity of the cross-peak to the associated diagonal peaks, one can quantify the coupling strength. These advantages of 2D spectroscopy allow us to identify the non-local coupling between HH and LH excitons in a disordered QW, which was largely unexplored previously.

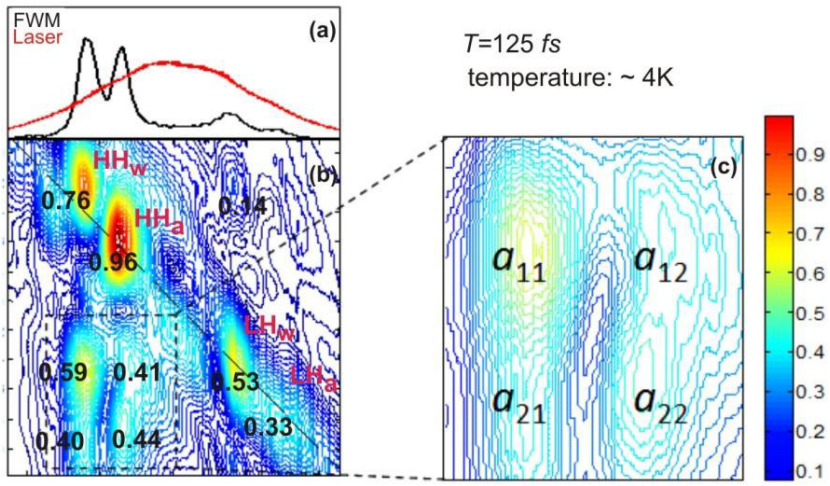

Figure 4. (a) FWM and (b) amplitude 2D spectra from the 8.4 nm QW. Co-linearly polarized excitation pulses are used. (c) Zoom-in view of the coupling matrix in the 2D spectrum. The amplitude spectrum is normalized to the maximal field amplitude. The amplitude of each peak in the 2D is explicitly labeled.

The measured one-dimensional FWM spectra and the amplitude 2D spectrum from the 8.4 nm QW is shown in figures 4(a) and (b). In the 2D spectrum, four diagonal peaks are identified as HH_w, HH_a, LH_w and LH_a, respectively. Their spectral positions along the emission frequency axis align with those resonances in the more familiar 1D FWM spectrum. In addition to these diagonal peaks, four cross-peaks are clearly present in the lower left quadrant of the 2D spectrum, which include the critical information on coherent coupling. We note that the cross-peaks in the upper right quadrant are largely missing. This asymmetry of the coupling matrix in 2DFTS has been reported in previous experiments [29] and may arise from many-body interactions. We replotted this coupling matrix in figure 4(c) and labeled each peak. The cross-peaks α_{11} and α_{22} correspond to the HH–LH coupling for excitons residing in the same QW regions. This type of coupling is expected and has been investigated extensively using conventional pump–probe spectroscopy, FWM and 2DFTS more recently [10, 29, 30]. In the simplest model, this type of HH–LH coherence can be described by Raman coherence between the two excited states that share a common ground state in a three-level V system.

The other two cross-peaks, labeled as α_{12} and α_{21}, correspond to HH–LH coupling for exciton coupling residing in different regions of the QW. Curiously, non-local coupling among the same type of excitons (i.e. HH–HH and LH–LH) are absent. One may naively expect that non-local LH–LH coupling should appear due to the lighter effective mass of LH excitons before the mixed-type exciton couplings occur. This type of non-local, mixed-type exciton coupling (i.e. non-local HH–LH coupling) has never been identified explicitly in previous experiments.

In contrast to conventional spectroscopy methods, such as quantum beats, the quantum mechanical pathways associated with coupling between different resonances are isolated as cross-peaks in the 2D spectrum, the intensity of which is directly related to coupling strength. The amplitude of each peak is labeled in figure 4(b). In the simplest model, the strongest possible coupling should yield a cross-peak amplitude to be the geometric average of the diagonal peak intensities, assuming that both resonances involved are excited equally. Not only is the

non-local, mixed-type exciton coupling present, but such coupling is very strong and comparable with coupling between HH–LH excitons residing in the same region of the QW.

4. Theoretical calculation based on the single defect model

We model the coherent nonlinear response from the disordered QW using a generalization of the semiconductor optical response theory within the $\chi^{(3)}$ approximation [40–43]. The equation of motion of the exciton nonlinear polarization $P^{(3)}(\boldsymbol{R}, t)$ can be written as (in units with $\hbar = 1$)

$$\left(\mathrm{i}\frac{\partial}{\partial t} + \mathrm{i}\gamma_\sigma - \hat{H}_\sigma(\boldsymbol{R})\right) P_\sigma^{(3)}(\boldsymbol{R}, t) = F_\sigma^{(3)}(\boldsymbol{R}, t). \tag{2}$$

Here $\boldsymbol{\sigma} = (\sigma, s)$ is a combined spin index describing the spin states of the hole, σ, and the electron, s, constituting the exciton; $\sigma = \pm 3/2$ and $\pm 1/2$ correspond to HH and LH, respectively; $\boldsymbol{R}$ is the spatial coordinates of the exciton center of mass. The interface fluctuations in the QW are accounted for by an effective disordered potential $W_\sigma(\boldsymbol{R})$ in the Hamiltonian of the exciton center of mass

$$\widehat{H}_\sigma(\boldsymbol{R}) = \omega_\sigma - \frac{1}{2M_\sigma}\nabla_{\boldsymbol{R}}^2 + W_\sigma(\boldsymbol{R}),$$

where M_σ is the exciton total mass and ω_σ is the exciton energy in an ideal QW [31, 44].

The driving term in equation (2) accounts for the interaction between excitons and is determined by many-body correlations [45–47]. Assuming that the intensity of the external excitation is not too high so that the effect of Pauli blocking can be neglected, and invoking the short-memory approximation, which neglects biexciton effects, we can present the driving term in the form

$$F_\sigma^{(3)}(\boldsymbol{R}, t) = -\frac{1}{2}\int \mathrm{d}\boldsymbol{R}_{1,2,3}\beta_{\sigma,\sigma_1}^{\sigma_2,\sigma_3}(R, R_1, R_2, R_3)p_{\sigma_1}^*(\boldsymbol{R}_1, t)p_{\sigma_2}(\boldsymbol{R}_2, t)p_{\sigma_3}(\boldsymbol{R}_3, t), \tag{3}$$

where summation over repeated spin indices is implied. Here the effective four-point potential β describes the Coulomb interaction and $p_\sigma(\boldsymbol{R}, t)$ are exciton linear polarizations. The latter are governed by equations of the same form as equation (2), but with the driving force determined by the external field, $F_\sigma^{(1)}(\boldsymbol{R}, t) = \vec{d}_\sigma \cdot \vec{E}(\boldsymbol{R}, t)$, where $\vec{E}$ is the electric field of the external excitation and $\vec{d}_\sigma$ is the matrix element of the dipole moment taken between the conduction and valence bands specified by the spin index $\boldsymbol{\sigma}$.

For our purpose of calculating coherent response along a phase-matched direction, it is sufficient to take the statistical average of the disordered potentials and to model the disordered potentials as circular defects of the same radius r_d. In addition, due to low spatial density of defects, we neglect multiple scattering between different defects. The disorder potential is thus simplified as $W_\sigma(\boldsymbol{R}) = \sum_m w_\sigma(\boldsymbol{R} - \boldsymbol{r}_m)$, where $\boldsymbol{r}_m$ is the position of mth defect, where $w_\sigma(\boldsymbol{r}) = -V_\sigma$ if $|\boldsymbol{r}| < r_\mathrm{d}$ and 0 otherwise.

To simplify our theory that models excitons of different masses, we adopt two additional approximations. Firstly, we take into account that the effective potential β in equation (3) is of the van der Waals type and decays fast with distance ($\propto 1/r^6$) and, thus, we treat it as a contact interaction: $\beta_{\sigma,\sigma_1}^{\sigma_2,\sigma_3}(R, R_1, R_2, R_3) = \beta_{\sigma,\sigma_1}\delta_{\sigma,\sigma_2}\delta_{\sigma_1,\sigma_3}\delta(R - R_1)\delta(R - R_2)\delta(R_1 - R_3)$, where we have taken into account the spin selection rules [45, 48]. Secondly, we retain only resonant

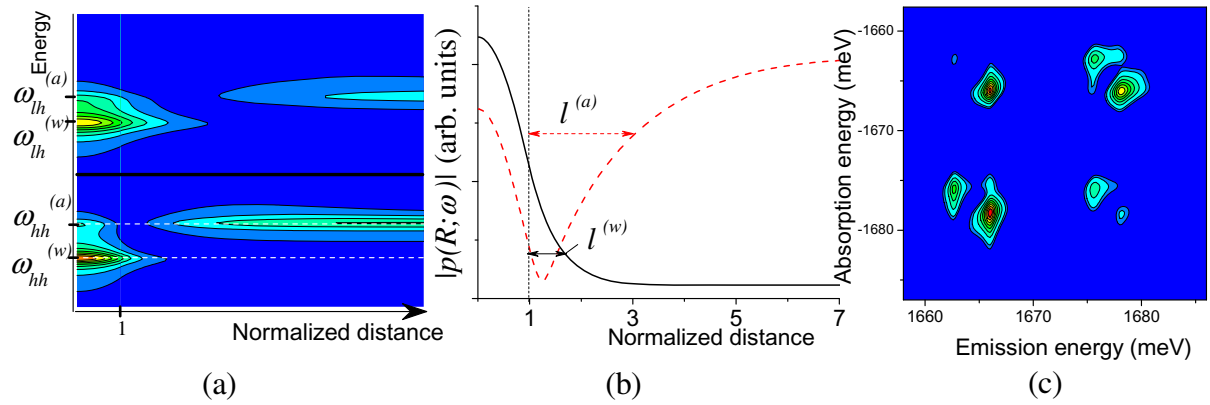

Figure 5. (a) The linear exciton polarization for HH (lower panel) and LH (upper panel) excitons as functions of frequency (vertical axis) and distance from the center of the defect (horizontal axis). $\boldsymbol{\omega}_{\mathbf{HH}}^{(\mathrm{w})}$ and $\boldsymbol{\omega}_{\mathbf{LH}}^{(\mathrm{w})}$ on the frequency axis mark the energies of HH and LH excitons bound to the defect, $\boldsymbol{\omega}_{\mathbf{HH}}^{(\mathrm{a})}$ and $\boldsymbol{\omega}_{\mathbf{LH}}^{(\mathrm{a})}$ correspond to the energies of excitons in the average QW thickness regions. (b) Typical distance dependence of the linear exciton polarization near the resonance frequencies corresponding to a bound state (solid line) residing in the wider regions of the QW and a state in regions of average thickness (dashed line, scaled by a factor of 2 for better presentation). The distance is normalized by the radius of the defect; the vertical dashed line shows the boundary of the defect. The coordinate dependence has qualitatively the same form for HH and LH excitons, therefore, we depict them only for HH excitons obtained as cuts of the linear response shown in part (a) along white dashed lines. (c) 2D Fourier spectrum calculated within the model of independent circular defects.

contributions to the 2D spectrum. Employing these assumptions, we find that the nonlinear polarization is given by

$$P_{\boldsymbol{\sigma}}^{(\mathrm{FWM})}(\omega_t,\omega_\tau)\sim n\sum_{\boldsymbol{\sigma}'}\beta_{\boldsymbol{\sigma},\boldsymbol{\sigma}'}\sum_{i,j=\{\mathrm{w,a}\}}\frac{\alpha_{j,k}(\boldsymbol{\sigma},\boldsymbol{\sigma}')}{\left(\omega_\tau+\omega_{\boldsymbol{\sigma}'}^{(j)}-\mathrm{i}\gamma_{\boldsymbol{\sigma}'}\right)\left(\omega_t-\omega_{\boldsymbol{\sigma}}^{(k)}+\mathrm{i}\gamma_{\boldsymbol{\sigma}}\right)\left(\omega_t-\omega_{\boldsymbol{\sigma}}^{(k)}+\mathrm{i}\gamma_{\boldsymbol{\sigma}}+2\mathrm{i}\gamma_{\boldsymbol{\sigma}'}\right)},$$

where n is the concentration of defects and the summation over $\boldsymbol{\sigma}'$ runs over all bright excitons, $\omega_{\boldsymbol{\sigma}}^{(\mathrm{w})}$ and $\omega_{\boldsymbol{\sigma}}^{(\mathrm{a})}$ are energies of excitons residing in the wider and average thickness regions, respectively. Parameters

$$\alpha_{j,k}(\boldsymbol{\sigma},\boldsymbol{\sigma}')\sim\frac{1}{A}\int_A \mathrm{d}\boldsymbol{R}\left|p_{\boldsymbol{\sigma}'}\left(\boldsymbol{R},\omega_{\boldsymbol{\sigma}'}^{(j)}\right)\right|^2\left|p_{\boldsymbol{\sigma}}\left(\boldsymbol{R},\omega_{\boldsymbol{\sigma}}^{(k)}\right)\right|^2$$

describe the spatial overlap of the linear responses at frequencies $\omega_{\boldsymbol{\sigma}'}^{(j)}$ and $\omega_{\boldsymbol{\sigma}}^{(k)}$, where A is the area per defect (the area of the QW divided by the number of defects).

The amplitude of each peak in the 2D spectrum depends on the overlap parameters $\alpha_{j,k}$, which, in turn, are determined by the linear polarization of the exciton resonances. The exciton linear polarization $p_{\boldsymbol{\sigma}}(\boldsymbol{R},t)$ of both HH and LH excitons near a circular defect as a function of frequency and the distance to the defect center is shown in figure 5(a). It is evident that exciton

pairs occupying the same regions (HH_w–LH_w and HH_a–LH_a) have the strongest overlap, and thus, lead to clear cross-peaks (α_{11} and α_{22}) in the calculated 2D spectrum in figure 5(c) as expected.

The presence of the non-local coupling between mixed-type excitons, in particular the cross-peak α_{12}, and the absence of the cross-peaks between excitons of the same type, can be explained by examining the overlap of linear response functions just outside the defect. For the bound state, $p_\sigma(\boldsymbol{R}, \omega_\sigma^{(w)})$ decays exponentially outside the defect (solid line in figure 5(b)) with the decay length $l_\sigma^{(w)} \sim 1/\sqrt{2M_\sigma \Delta_\sigma}$, where $\Delta_\sigma = \omega_\sigma^{(a)} - \omega_\sigma^{(w)}$. The linear response function of the delocalized states (dashed line in figure 5(b)) is somewhat counterintuitive. The amplitude is appreciable inside the defect, reaches a minimal near the boundary of the defect, and then grows logarithmically away from the defect. We can define the width of the dip as $l_\sigma^{(a)} \sim 1/\sqrt{2M_\sigma \gamma_\sigma}$. The overlap of the bound exciton $\boldsymbol{\sigma}$ and the delocalized exciton $\boldsymbol{\sigma}'$ is proportional to

$$\eta_{\sigma,\sigma'} = \frac{l_\sigma^{(w)}}{l_{\sigma'}^{(a)}} = \sqrt{\frac{M_{\sigma'}\gamma_{\sigma'}}{M_\sigma \Delta_\sigma}}.$$

For excitons of the same type $\eta_{\sigma,\sigma} \approx \sqrt{\gamma_\sigma/\Delta_\sigma}$, and one has $\eta_{\sigma,\sigma} < 1$ when the resonances are spectrally well resolved. The small $\eta_{\sigma,\sigma}$ suggests negligible coupling as evidenced by the lack of cross-peak between HH_w and HH_a (or between LH_w and LH_a) in the simulated 2D spectrum. When one considers excitons of different types, however, the factor $M_{\sigma'}/M_\sigma$ may be large and thus overcome the spatial and spectral separation between the exciton states. As a result, the coupling between HH_a and LH_w is enhanced due to the high-mass ratio $M_{HH}/M_{LH} \approx 4$ in GaAs and is manifested as the cross-peak α_{12} in both the simulated and measured 2D spectra.

The cross-peak α_{21} observed in the experiment is not prominent in the simulated spectrum. Nevertheless, the coupling is manifested as a vertical elongation of the cross-peak α_{11} in figure 5(c). We resort to a different argument to explain the presence of this cross-peak. Because of the smaller effective mass, the LH_a penetrates into the defect and partially overlaps with the state HH_w, leading to the cross-peak α_{21}. Interestingly, the coupling between LH_w and LH_a is weaker than α_{21} and cannot be observed in either measured or simulated spectra because the amplitude of the linear response function of LH_w is smaller than that of HH_w due to its smaller dipole moment and faster dephasing time. Finally, we note that our simulated 2D spectrum did not fully account for the asymmetry of the coupling matrix, (i.e. the weak or missing cross-peaks in the upper right quadrant of the experimental 2D spectra), which is a many-body effect as noted in previous 2D studies [29].

5. Conclusion

In summary, we investigated coherent coupling among excitons in a single disordered QW using 2DFTS. We observed four different exciton resonances as HH and LH excitons residing in the wider and average thickness regions of the QW. Cross-peaks in the 2D spectrum allow us to identify the surprising non-local HH–LH coupling in addition to the expected HH–LH coupling between excitons residing in the same regions. Curiously, the non-local coupling between the same types of excitons (i.e. non-local HH–HH and LH–LH coupling) is absent. A complete theoretical treatment of coherent coupling among excitons in a disordered quantum system is not achievable at present. Alternatively, we relied on the single defect model to provide some intuitive understanding of a rather complicated problem.

Acknowledgments

We gratefully acknowledge financial support from the following sources: NSF DMR-0747822, Welch Foundation F-1662, ARO-W911NF-08-1-0348 and the Alfred P Sloan Foundation. MNL acknowledges support from NSF (grant no. ECCS-0901784), AFOSR (grant no. FA9550-09-1-0450) and NSF (grant no. ECCS-1128597).

References

[1] Chemla D S and Shah J 2001 *Nature* **411** 549
[2] Cundiff S T 2008 *Opt. Express* **16** 4639
[3] Leo K, Wegener M, Shah J, Chemla D S, Göbel E O, Damen T C, Schmitt-Rink S and Schäfer W 1990 *Phys. Rev. Lett.* **65** 1340
[4] Kim D-S, Shah J, Damen T C, Schäfer W, Jahnke F, Schmitt-Rink S and Köhler K 1992 *Phys. Rev. Lett.* **69** 2725
[5] Wang H, Ferrio K, Steel D G, Hu Y Z, Binder R and Koch S W 1993 *Phys. Rev. Lett.* **71** 1261
[6] Shacklette J M and Cundiff S T 2002 *Phys. Rev.* B **66** 045309
[7] Hochstrasser R M 2007 *Proc. Natl Acad. Sci. USA* **104** 14189
[8] Mukamel S 2000 *Annu. Rev. Phys. Chem.* **51** 691
[9] Cundiff S T, Zhang T H, Bristow A D, Karaiskaj D and Dai X C 2009 *Acc. Chem. Res.* **42** 1423
[10] Li X, Zhang T, Borca C N and Cundiff S T 2006 *Phys. Rev. Lett.* **96** 057406
[11] Stone K W, Gundogdu K, Turner D B, Li X Q, Cundiff S T and Nelson K A 2009 *Science* **324** 1169
[12] Karaiskaj D, Bristow A D, Yang L J, Dai X C, Mirin R P, Mukamel S and Cundiff S T 2010 *Phys. Rev. Lett.* **104** 117401
[13] Davis J A, Hall C R, Dao L V, Nugent K A, Quiney H M, Tan H H and Jagadish C 2011 *J. Chem. Phys.* **135** 044510
[14] Li X Q, Zhang T H, Mukamel S, Mirin R P and Cundiff S T 2009 *Solid State Commun.* **149** 361
[15] Luo M S C, Shun Lien C, Planken P C M, Brener I, Roskos H G and Nuss M C 1994 *IEEE J. Quantum Electron.* **30** 1478
[16] Feuerbacher B F, Kuhl J, Eccleston R and Ploog K 1990 *Solid State Commun.* **74** 1279
[17] Göbel E O, Leo K, Damen T C, Shah J, Schmitt-Rink S, Schäfer W, Müller J F and Köhler K 1990 *Phys. Rev. Lett.* **64** 1801
[18] Leo K, Damen T C, Shah J, Gobel E O and Kohler K 1990 *Appl. Phys. Lett.* **57** 19
[19] Joschko M, Woerner M, Elsaesser E, Binder E, Hey R, Kostial H and Ploog K 1997 *Phys. Rev. Lett.* **78** 737
[20] Ferrio K B and Steel D G 1998 *Phys. Rev. Lett.* **80** 786
[21] Koch M, Feldmann J, Göbel E O, Thomas P, Shah J and Kohler K 1993 *Phys. Rev.* B **48** 11480
[22] Euteneuer A *et al* 1999 *Phys. Rev. Lett.* **83** 2073
[23] Phillips M and Wang H L 1999 *Solid State Commun.* **111** 317
[24] Kasprzak J, Patton B, Savona V and Langbein W 2011 *Nature Photon.* **5** 57
[25] Takagahara T 1985 *Phys. Rev.* B **31** 6552
[26] Engel G S, Calhoun T R, Read E L, Ahn T K, Mancal T, Cheng Y C, Blankenship R E and Fleming G R 2007 *Nature* **446** 782
[27] Ishizaki A and Fleming G R 2011 *J. Phys. Chem.* B **115** 6227
[28] Collini E, Wong C Y, Wilk K E, Curmi P M G, Brumer P and Scholes G D 2010 *Nature* **463** 644
[29] Borca C N, Zhang T H, Li X Q and Cundiff S T 2005 *Chem. Phys. Lett.* **416** 311
[30] Zhang T H, Kuznetsova I, Meier T, Li X C, Mirin R P, Thomas P and Cundiff S T 2007 *Proc. Natl Acad. Sci. USA* **104** 14227
[31] Castella H and Wilkins J W 1998 *Phys. Rev.* B **58** 16186
[32] Savona V and Langbein W 2006 *Phys. Rev.* B **74** 075311

[33] Bimberg D, Christen J, Fukunaga T, Nakashima H, Mars D E and Miller J N 1987 *J. Vac. Sci. Technol.* B **5** 1191
[34] Gammon D, Shanabrook B V and Katzer D S 1991 *Phys. Rev. Lett.* **67** 1547
[35] Hu Y Z, Binder R, Koch S W, Cundiff S T, Wang H and Steel D G 1994 *Phys. Rev.* B **49** 14382
[36] Santos P V, Willatzen M, Cardona M and Cantarero A 1995 *Phys. Rev.* B **51** 5121
[37] Bracker A S *et al* 2005 *Phys. Rev.* B **72** 035332
[38] Gammon D, Snow E S, Shanabrook B V, Katzer D S and Park D 1996 *Phys. Rev. Lett.* **76** 3005
[39] Bristow A D, Karaiskaj D, Dai X, Zhang T, Carlsson C, Hagen K R, Jimenez R and Cundiff S T 2009 *Rev. Sci. Instrum.* **80** 073108
[40] Lindberg M, Hu Y Z, Binder R and Koch S W 1994 *Phys. Rev.* B **50** 18060
[41] Victor K, Axt V M and Stahl A 1995 *Phys. Rev.* B **51** 14164
[42] Schäfer W, Kim D S, Shah J, Damen T C, Cunningham J E, Goossen K W, Pfeiffer L N and Köhler K 1996 *Phys. Rev.* B **53** 16429
[43] Kwong N H, Takayama R, Rumyantsev I, Kuwata-Gonokami M and Binder R 2001 *Phys. Rev.* B **64** 045316
[44] Zimmermann R and Runge E 1997 *Phys. Status Solidi* a **164** 511
[45] Östreich T, Schönhammer K and Sham L J 1998 *Phys. Rev.* B **58** 12920
[46] Savasta S, Di Stefano O and Girlanda R 2003 *Phys. Rev. Lett.* **90** 096403
[47] Erementchouk M, Leuenberger M N and Sham L J 2007 *Phys. Rev.* B **76** 115307
[48] Erementchouk M, Turkowski V and Leuenberger M N 2012 *Advances in Quantum Field Theory* ed S Ketov (Rijeka, Croatia: InTech)